Spectral line shapes in systems undergoing continuous frequency modulation

Cite as: J. Chem. Phys. **105**, 2686 (1996); https://doi.org/10.1063/1.472132
Submitted: 15 December 1995 . Accepted: 06 May 1996 . Published Online: 31 August 1998

Paras M. Agrawal, Dan C. Sorescu, Ronald D. Kay, Donald L. Thompson, Lionel M. Raff, J. Brian Conrey, and A. Keith Jameson

Spectral line shapes in systems undergoing continuous frequency modulation

Paras M. Agrawal,[a] Dan C. Sorescu,[b] Ronald D. Kay,[c] Donald L. Thompson, and Lionel M. Raff
Department of Chemistry, Oklahoma State University, Stillwater, Oklahoma 74078

J. Brian Conrey
Department of Mathematics, Oklahoma State University, Stillwater, Oklahoma 74078

A. Keith Jameson
Department of Chemistry, Loyola University, Chicago, Illinois 60626

(Received 15 December 1995; accepted 6 May 1996)

The power spectrum line shapes for oscillators undergoing a continuous modulation of the vibrational frequency are investigated. It is shown that the single, sharp line normally characteristic of such systems broadens and exhibits a wealth of fine structure components. The characteristic fine structure pattern is one of decreasing amplitude and spacing. This continuous frequency modulation (CFM) effect has been examined for a series of model oscillators that includes harmonic systems with linear and exponential variation of the frequency without amplitude damping, a harmonic system with exponential damping of both the resonant frequency and the amplitude, and a Morse oscillator whose kinetic energy is being exponentially damped. An analytic expression for the power spectrum of a harmonic oscillator whose frequency is varying linearly with time is derived. This result demonstrates that the position of the fine structure extrema depends linearly upon the initial oscillator frequency and the square root of the absolute value of the modulation rate. The peak-to-peak spacing is shown to be proportional to the square root of the absolute value of the modulation rate. It is suggested that the CFM effect is the fundamental explanation of many previous empirical observations concerning power spectra. The CFM effect for a harmonic system with an exponentially modulated frequency is very similar to that observed for linear modulation. When amplitude depression is included, there is a significant intensity decrease of many of the spectral lines. Investigation of a Morse oscillator shows that energy transfer in an anharmonic system produces a CFM effect. By assuming that the analytic result for a harmonic oscillator with a linear modulation is transferable to the anharmonic case, an expression is obtained that relates the peak-to-peak fine structure spacing to the Morse potential parameters, the initial oscillator energy and the IVR rate coefficient. An experimental example of a CFM effect is presented by taking an NMR spectrum of H_2O and $HCCl_3$ in $DCCl_3$ while the main $\mathbf{B_0}$ field is varying with time. The CFM effect is used to extract energy transfer rate coefficients for a diatomic molecule isolated in an argon matrix at 12 K and for total IVR rate coefficients for relaxation of the N═O and O–H local modes in *cis*-HONO. It is also shown that instantaneous energy transfer rates in small molecules can be determined by using local frequency analysis to compute the temporal variation of the CFM band spacings. It is concluded that line shape analysis can be effectively used as a probe of energy transfer rates. [S0021-9606(96)00131-6]

I. INTRODUCTION

Trajectory and molecular dynamics (MD) methods are the most frequently used and powerful methods for the investigation of the dynamical behavior of many-body systems. These techniques have been employed to calculate reaction rate coefficients, cross sections, diffusion rates, product energy partitioning, inter- and intramolecular energy transfer rates, and relaxation rates in both gas and condensed phases.[1] When combined with Monte Carlo procedures, MD methods frequently permit complex reaction mechanisms to be determined in detail.[2]

A great deal of the dynamical information available from the results of an MD calculation is contained in the computed power spectrum. A power spectrum for a given coordinate, q, may be computed by taking the Fourier transform of either an autocorrelation function, $C_q(\tau)$, or by transforming the coordinate itself.[3] The autocorrelation function is given by

$$C_q(\tau)=\lim_{T\to\infty}\left[(T)^{-1}\int_0^T q(t)q(t+\tau)dt\right]. \tag{1}$$

The power spectrum of $C_q(\tau)$ is then obtained from

[a]Present address: School of Studies in Physics, Vikram University, Ujjain MP 456 010, India.
[b]Present address: Department of Chemistry, University of Pittsburgh, Pittsburgh, PA 15260.
[c]Present address: Department of Chemistry, Gordon College, 255 Grapevine Road, Wenham, MA 01984.

 0021-9606/96/105(7)/2686/15/$10.00

$$I_c(\omega)=(2\pi)^{-1}\left|\int_{-\infty}^{\infty}C_q(\tau)\exp\{i\omega\tau\}d\tau\right|^2. \tag{2}$$

A power spectrum obtained from a direct transformation of the coordinate is given by

$$I_q(\omega)=(2\pi)^{-1}\left|\int_{-\infty}^{\infty}q(t)\exp\{i\omega t\}dt\right|^2. \tag{3}$$

In principle, $I_c(\omega)$ and $I_q(\omega)$ contain the same information. However, this is not always apparent. $I_c(\omega)$ and $I_q(\omega)$ differ in that $I_c(\omega)$ is the square of $I_q(\omega)$. This difference means the two quantities emphasize the features of the dynamics in different ways. The magnitude of $I_q(\omega^*)$ is proportional to the modulus of the Fourier component of $q(t)$ with frequency ω^*, whereas the magnitude of $I_c(\omega^*)$ depends upon the square of this modulus. As a result, a power spectrum obtained from $I_c(\omega)$ will emphasize the major frequency components of the spectrum at the expense of the smaller peaks. If the objective of the analysis is to obtain the major fundamental frequencies associated with the dynamics, this result is ideal. If, however, the objective is to monitor the onset of smaller frequency components, $I_q(\omega)$ is a more useful diagnostic tool.

In their original investigations, Noid *et al.*[3] examined power spectra for two model Hamiltonians and demonstrated that sharp line spectra for fundamentals, overtones, and combination bands result whenever quasiperiodic dynamics exists. In contrast, ergodic dynamics was shown to lead to more broadened spectra containing many smaller peaks. Smith and Shirts[4] computed averaged power spectra for state-specific excitation of HCN and found that the ensemble-averaged spectra do not exhibit the expected broadening and grassiness with increasing internal energy, but that the spectra of individual trajectories do. Dumont and Brumer[5] have pointed out that the observation of simple vs complex power spectra provide distinguishing characteristics. For a Henon–Heiles model and for the three-body NaClK system, the statistical analysis of power spectra at a fixed energy were shown to provide an adequate method for distinguishing chaotic and quasiperiodic motions. Chang *et al.*[6] were able to demonstrate that the qualitative appearance of the power spectrum can be used as a diagnostic tool to assess the statistical character of a system. The presence of a diffuse spectrum exhibiting a nearly complete loss of isolated structures indicates that the dissociation dynamics of the molecule will be well described by statistical theories. If, however, the power spectrum maintains its discrete, isolated character, the opposite conclusion is suggested.

In this paper, we demonstrate that the above observations are a consequence of a general interference phenomenon that exists for all systems whose resonant frequencies are a continuously varying function of time. In Sec. II, we treat a simple, modified harmonic model system for which it is possible to compute the power spectra $I_q(\omega)$ analytically. The results demonstrate the nature of the power spectra expected for a continuous frequency modulated (CFM) system. We infer that it is the CFM effect that gives rise to the qualitative observations made by Noid *et al.*,[3] Smith and Shirts,[4] Dumont and Brumer,[5] and Chang *et al.*[6] The analysis shows that the band spacings of the CFM interference pattern can be used to extract the frequency modulation rate. Section III reports similar numerical studies on a CFM Morse oscillator. In Sec. IV, we provide direct experimental verification of the CFM effect. The results of MD simulations of the vibrational relaxation of a matrix-isolated diatomic molecule and of intramolecular vibrational relaxation (IVR) of *cis*-HONO are presented in Sec. V. The relaxation rates are computed from the band spacings produced by the CFM effect. The accuracy of the method is assessed by direct comparison of these rates with results obtained from first-order decay plots of the vibrational energy. In Sec. VI, we demonstrate how local frequency analysis can be used in conjunction with the CFM effect to investigate energy transfer rates in small molecules. The paper concludes with a summary of our findings.

II. HARMONIC MODELS

It is well known that the shapes of spectral lines often contain important information about the system under consideration. Recent articles by Miller[7] and by Wood and Strauss[8] describe the connection between the absorption line width and the IVR and reaction rates. Following Kubo,[9] both Wood and Strauss,[8] and Saven and Skinner[10] have discussed the modulation process in terms of a dimensionless parameter, κ, called the ''Kubo parameter.'' These reviews show that the form of the absorption function is well known for the extreme values $\kappa\gg1$ or $\kappa\ll1$. However, for intermediate values of κ, these studies state that complicated line shapes result.

Kubo considers an oscillator having angular frequency $\omega(t)$ such that

$$\omega(t)=\omega_0+\Omega(t), \tag{4}$$

where ω_0 is a constant and $\Omega(t)$ is a random variable with zero mean that is described by the stationary Gaussian probability distribution

$$P(\Omega)=(2\pi\Delta^2)^{-1/2}\exp[-\Omega^2/(2\Delta^2)] \tag{5}$$

and the time correlation function

$$\langle\Omega(0)\Omega(t)\rangle=\Delta^2\exp[-|t|/\tau_c]. \tag{6}$$

Thus Δ is the ''modulation amplitude,'' that is, the root mean square of the angular frequency fluctuations while τ_c is the ''modulation time,'' that is, the characteristic time that frequency fluctuations persist. The dimensionless Kubo parameter is defined to be

$$\kappa=\tau_c\Delta. \tag{7}$$

Saven and Skinner[10] have shown that for the condition $\kappa\gg1$, the absorption line shape becomes Gaussian,

$$I(\omega)=(2\pi\Delta^2)^{-1/2}\exp[-(\omega-\omega_0)^2/(2\Delta^2)]. \tag{8}$$

This gives a half width at half height of the order of Δ. In the limit $\kappa\ll1$, a Lorentzian line shape results,

$$I(\omega)=(\tau_c\Delta^2/\pi)/[(\omega-\omega_0)^2+(\tau_c\Delta^2)^2]. \tag{9}$$

The half width at half height for this line is on the order of $\tau_c\Delta^2$ or $\kappa\Delta$ which is considerably less than Δ. The analysis presented by Saven and Skinner[10] states that for intermediate values of κ, more complicated line shapes result.

In MD simulations, bonding potentials are always anharmonic. Frequently, Morse functions,

$$V(r)=D[1-\exp\{-\beta(r-r_e)\}]^2, \tag{10}$$

are employed to represent such interactions. In Eq. (10), D, β, and r_e are parameters which determine the potential well depth, curvature and potential minimum, respectively, and r is the bond length. The fundamental vibrational frequency for a Morse oscillator is given by[11]

$$\omega=\beta(2D/\mu)^{1/2}[1-(E/D)]^{1/2}, \tag{11}$$

where μ is the reduced mass of the oscillator. Consequently, if intra- or intermolecular vibrational energy transfer occurs, we would see a continuous modulation of the oscillator frequency. To be certain, the variation in frequency would not be described by a Gaussian distribution as assumed by Kubo.[9] However, we still might expect to see simple line shapes for the limiting cases $\kappa\gg1$ and $\kappa\ll1$ and more complex shapes for intermediate values of κ. In many MD simulations of intramolecular energy transfer, we find that the angular frequency variations are on the order of 600 cm^{-1}. These variations usually occur on a time scale of 1 ps. We therefore expect κ to be about 18. For this intermediate value, we would expect complicated line shapes.

To provide a simple model of the type of line shapes to be expected in a power spectrum of an oscillator undergoing continuous frequency modulation, we first consider a modified ''harmonic'' oscillator for which the displacement, $f(t)$, is given by

$$f(t)=r(t)-r_e=A\ \sin[\omega(t)t] \quad \text{for } 0\leqslant t\leqslant T \quad \text{and } f(t)=0 \text{ otherwise}, \tag{12}$$

where A is a constant and $\omega(t)$ is defined by

$$\omega(t)=2\pi\nu_0(1-kt)=2\pi\nu_0-2\pi\alpha t, \tag{13}$$

with ν_0, k, and T all positive. That is, we have a linear modulation with time. The complex nature of the power spectrum associated with the oscillator described by Eqs. (12) and (13) is shown in Fig. 1(B) for the case $A=2.0$ Å, $\nu_0=2.0$ t.u.$^{-1}$ and $k=0.0003$ t.u.$^{-1}$ where 1 t.u.$=1.018\times10^{-14}$ s. This power spectrum was obtained using a fast Fourier transform routine on a data set comprising 4096 values of $f(t)$ evaluated at equally spaced times from zero to 500 t.u. As can be seen, the spectrum is a broad band replete with fine structure components whose spacing first decreases and then increases as $\omega(t)$ decreases. Repeated calculations show that the peak-to-peak spacings of the fine structure increase as α increases. This suggests that the fine structure spacing might be used as a probe of the rate at which the frequency is being modulated.

An analytic expression for the power spectrum shown in Fig. 1(B) can be obtained from the Fourier transform

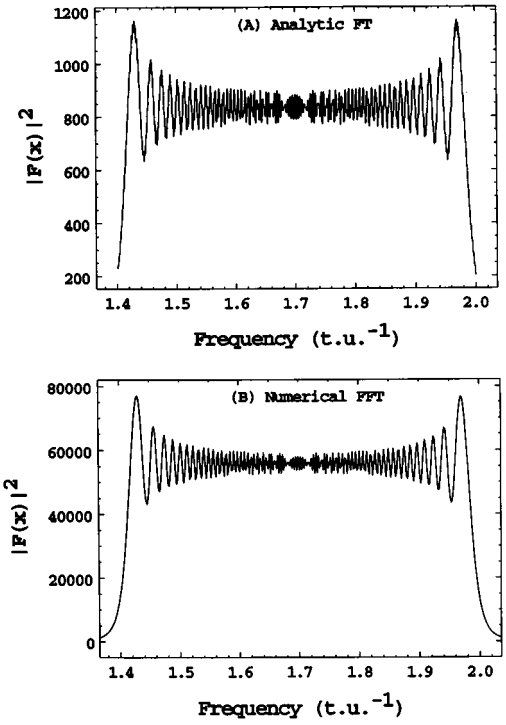

FIG. 1. Power spectrum for the oscillator defined by Eqs. (12) and (13) in the text with $A=2.0$ Å. $\nu_0=2.0$ t.u.$^{-1}$, $k=0.0003$ t.u.$^{-1}$ and $T=500.0$ t.u. (1 t.u.$=1.018\times10^{-14}$ s). (A) Computed from analytic Fourier transform given in Eq. (27). (B) Computed with a fast Fourier transform (FFT) method using 4096 equally-spaced values of $r(t)$ from 0 to 500 t.u.

$$F(x)=\int_{-\infty}^{\infty}f(t)e[xt]dt, \tag{14}$$

where we define

$$e[z]\equiv\exp[2\pi iz]. \tag{15}$$

We will assume that $x\geqslant0$ as it is clear that $F(-x)=F(x)$. Writing Eq. (12) as a sum of exponentials gives

$$F(x)=(i)^{-1}\int_0^T\{e[(x+\nu_0)t]e[-\alpha t^2] - e[(x-\nu_0)t]e[\alpha t^2]\}dt, \tag{16}$$

provided we take the wave amplitude $A=2$ Å. The first part of the integral in Eq. (16) is negligible relative to the second part. This may be seen as follows: Suppose $p(t)$ is a continuous, differentiable real valued function on the interval $[t_1,t_2]$ and that $p'(t)$ is either monotonically increasing or decreasing on this interval. If $|p'(t)|\geqslant M>0$ for $t_1\leqslant t\leqslant t_2$, then it may be shown[12] that

$$\left|\int_{t_1}^{t_2}\exp[ip(t)]dt\right|\leqslant4/M. \tag{17}$$

We may apply this Lemma to the first part of the integral in Eq. (16) by taking

$$p(t)=2\pi[(x+\nu_0)t-\alpha t^2]. \tag{18}$$

This gives $p'(t)=2\pi[(x+\nu_0)-2\alpha t]$. Since $\alpha>0$, $p'(t)$ decreases monotonically with time. Thus if we take t to have its maximum value of T, $p'(t)$ will be a minimum and we are assured that $|p'(t)|\geqslant M>0$ provided we take $M=2\pi[(x+\nu_0)-2\alpha T]$ and $(x+\nu_0)>2\alpha T$. In physically real cases, this latter inequality is expected to hold since $\omega(t)$ will always be positive. Consequently, we have

$$\left|\int_0^T e[(x+\nu_0)t]e[-\alpha t^2]dt\right|\leqslant 4\{2\pi[(x+\nu_0)-2\alpha T]\}^{-1}. \tag{19}$$

If $T<C/2k$ where $C>0$, we have $\{2\pi[(x+\nu_0)-2\alpha T]\}>2\nu_0(1-C)$. Hence, Eq. (19) can be written as

$$\left|\int_0^T e[(x+\nu_0)t]e[-\alpha t^2]dt\right|\leqslant 4[2\nu_0(1-C)]^{-1}. \tag{20}$$

The second term in the integral of Eq. (16) is

$$F_2(x)=i\int_0^T e[(x-\nu_0)t]e[\alpha t^2]dt. \tag{21}$$

Since the derivative of the integrand of Eq. (21) increases monotonically with t, to use the above Lemma, we would need to take $M=2\pi(x-\nu_0)$ which becomes zero for $x=\nu_0$. Consequently, no finite upper bound for $F_2(x)$ can be obtained. If we define $-b=x-\nu_0$ and complete the square on the integrand for Eq. (21), we obtain

$$F_2(x)=i\int_0^T e[\alpha(t-b/(2\alpha))^2-b^2/(4\alpha)]dt. \tag{22}$$

For convenience, let $\theta=t-b/(2\alpha)$. Substitution into Eq. (22) gives

$$F_2(x)=ie[-b^2/(4\alpha)]\int_{-b/2\alpha}^{T-b/2\alpha} e[\alpha\theta^2]d\theta. \tag{23}$$

The substitution $\gamma=\alpha^{1/2}\theta$ transforms Eq. (23) into

$$F_2(x)=i\alpha^{-1/2}e[-b^2/(4\alpha)]\int_{-b/2\alpha^{1/2}}^{T\alpha^{1/2}-b/2\alpha^{1/2}} e[\gamma^2]d\gamma. \tag{24}$$

Now let

$$h(y,U)\equiv\int_{-y}^{U-y} e[\gamma^2]d\gamma=\int_0^y e[\gamma^2]d\gamma+\int_0^{U-y} e[\gamma^2]d\gamma$$
$$=H(y)+H(U-y), \tag{25}$$

where

$$H(z)\equiv\int_0^z e[\gamma^2]d\gamma. \tag{26}$$

$H(z)$ can be expressed in terms of the complex error function. In this notation, the Fourier transform of $f(t)$ may be written as

$$F(x)=F_2(x)+\Theta[2\nu_0(1-C)]^{-1}$$
$$=i\alpha^{-1/2}e[-b^2/4\alpha]h(b/2\alpha^{1/2},T\alpha^{1/2})$$
$$+\Theta[2\nu_0(1-C)]^{-1}$$
$$=i\alpha^{-1/2}e[-b^2/4\alpha]\{H(b/2\alpha^{1/2})$$
$$+H(T\alpha^{1/2}-b/2\alpha^{1/2})\}$$
$$+\Theta[2\nu_0(1-C)]^{-1}, \tag{27}$$

where Θ is some number satisfying the condition $|\Theta|\leqslant 1$.

If we ignore the final term in Eq. (27), the power spectrum will be given by $|F_2(x)|^2$. A plot of $|F_2(x)|^2$ for the specific case used above is shown in Fig. 1(A). Comparison with the FFT numerical result in Fig. 1(B) shows the two to be nearly identical except for the arbitrary scaling of the numerical result. The only significant difference between the two transforms is the presence of a series of small, superimposed maxima on the major bands of the analytic transform. It is shown in the following analysis that these small maxima are due to the $H(T\alpha^{1/2}-b/2\alpha^{1/2})$ term in Eq. (27). These features are lost in the FFT result due to the limited resolution of the numerical procedure.

The behavior of $|F(x)|^2$ depends primarily upon $|h(y,U)|^2$ in the range $0\leqslant y\leqslant U$ since outside this range the above Lemma may be used to show that the modulus of $F(x)$ is small. The fine structure seen in Fig. 1 demonstrates that $|F(x)|^2$ exhibits a series of extrema over the range of frequencies sampled. These extrema will correspond closely to those for $|H(y)|^2$. We therefore need to determine the location of these points. We begin by writing

$$|H(y)|^2=\int_0^y e[z^2]dz\int_0^y e[-u^2]du. \tag{28}$$

Application of Leibnitz's rule[13] gives

$$(d/dy)|H(y)|^2=2\Re\left\{e[y^2]\int_0^y e[-u^2]du\right\}$$
$$=2\Re\left\{\int_0^y e[y^2-u^2]du\right\}$$
$$=2\int_0^y \cos[2\pi(y^2-u^2)]du, \tag{29}$$

where the operator $\Re$ denotes the real part of the expression. With the substitution $\Gamma=u^2$, Eq. (29) becomes

$$\left(\frac{d}{dy}\right)|H(y)|^2=\int_0^{y^2}\Gamma^{-1/2}\cos[2\pi(y^2-\Gamma)]d\Gamma\equiv g(y^2), \tag{30}$$

where

$$g(s)=\int_0^s\Gamma^{-1/2}\cos[2\pi(s-\Gamma)]d\Gamma. \tag{31}$$

Equation (31) may be written more compactly by defining

$$s-\Gamma\equiv\sigma \tag{32}$$

and

$$\sigma\equiv\delta s. \tag{33}$$

Substitution into Eq. (31) yields

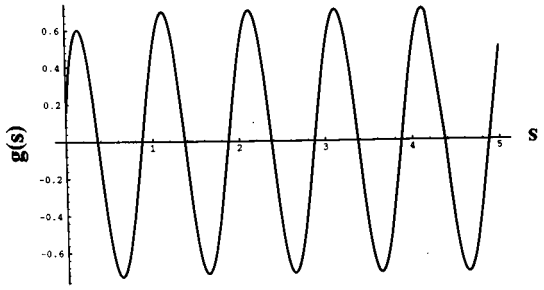

FIG. 2. $g(s)$ as a function of y for $0 \leqslant s \leqslant 5$. $g(s)$ is defined by Eq. (31) in the text.

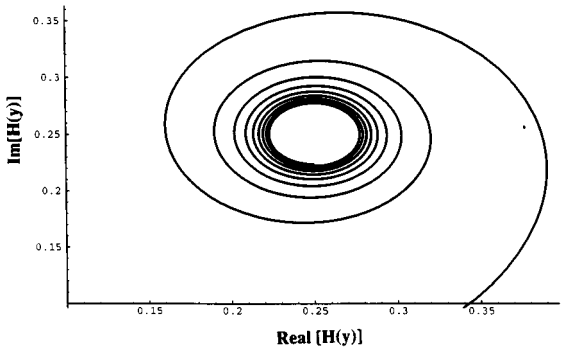

FIG. 3. Plot of $H(y)$ in the complex plane for real values of y over the range $0 \leqslant y \leqslant 3$. As y increases, $H(y)$ is seen to approach its limiting value of $(1+i)/4$.

$$g(s) = \int_0^s (s-\sigma)^{-1/2} \cos[2\pi\sigma]\, d\sigma$$

$$= s^{1/2} \int_0^1 (1-\delta)^{-1/2} \cos[2\pi s\delta]\, d\delta. \tag{34}$$

The extrema of $|F(x)|^2$ occur at the zeros of $g(y^2)$ which correspond to the zeros of $g(s)$. It can be shown[14] that if $f(t)$ is a positive, increasing function defined on the interval $0 \leqslant t \leqslant 1$ such that the integral, $\int_0^1 f(t)dt$, is finite, then the function

$$\int_0^1 f(t)\cos(zt)dt$$

has only real zeros. It therefore follows that $g(s)$ has only real zeros. It can be shown that the zeros of $g(s)$ are nearly uniformly spaced (see Fig. 2), with the distance between consecutive zeros approaching 1/2. The nth zero, excluding $s=0$, of $g(s)$ is essentially at $[n/2-1/8]$. Therefore, the number of zeros of $g(s)$ in the range $0 \leqslant s \leqslant Y$ will be about $2Y$ and the number of extrema of $|H(y)|^2$ in this range will be approximately $2Y^2$. Consequently, the number of maxima exhibited by $|H(y)|^2$ will be about Y^2. The successive zeros corresponding to maxima of $g(s)$ will be near 3/8, 11/8, 19/8,..., $(n-5/8)$, ..., so that the maxima of $|H(y)|^2$ will occur near $y=M(n)$ where $M(n)=(n-5/8)^{1/2}$ for $n=1,2,3,\cdots$. The change in the peak position is

$$dM(n) = dn/[2(n-5/8)^{1/2}], \tag{35}$$

which for large n approaches $1/[2n^{1/2}]$ for unit change in n. Therefore, the spacing between the successive maxima decreases monotonically with $n^{1/2}$.

Figure 2 shows a plot of $g(s)$ as a function of s over the range $0 \leqslant s \leqslant 5$. As can be seen, the zeros of $g(s)$ are nearly equally spaced. If we denote the successive zeroes of $g(s)$ as $s_i (i=1,2,3,\cdots)$, we find $s_1 = 0.365\cdots$, $s_2 = 0.878\cdots$, $s_3 = 1.373\cdots$. Hence, the corresponding extrema for $|H(y)|^2$ occur at $(0.365\cdots)^{1/2} = 0.604\cdots$, $(0.878\cdots)^{1/2} = 0.937\cdots$, and $(1.373)^{1/2} = 1.171\cdots$.

It is also instructive to consider the variation of $H(y)$ with y. As y increases without bound, we have

$$\lim_{y\to\infty} H(y) = (1+i)/4. \tag{36}$$

The graph of $H(y)$ for real y traces a curve that spirals around the point $(1+i)/4$ getting steadily closer as $y \to \infty$. The distance between $H(y)$ and $(1+i)/4$ is given by

$$D = \left| \int_y^\infty e[z^2]dz \right|. \tag{37}$$

The derivative of the square of D is[13]

$$\frac{dD^2}{dy} = -2\Re \int_y^\infty e[(z^2-y^2)]dz$$

$$= -2 \int_y^\infty \cos[2\pi(z^2-y^2)]dz. \tag{38}$$

Substitution of $u=z^2$ gives

$$\frac{dD^2}{dy} = -\int_{y^2}^\infty u^{-1/2} \cos[2\pi(u-y^2)]du. \tag{39}$$

If we let $u=wy^2$, Eq. (39) becomes

$$\frac{dD^2}{dy} = -y \int_1^\infty w^{-1/2} \cos[2\pi y^2(w-1)]dw. \tag{40}$$

Replacement of w with $(v+1)$ gives

$$\frac{dD^2}{dy} = -y \int_0^\infty (v+1)^{-1/2} \cos[2\pi y^2 v]dv. \tag{41}$$

If Eq. (41) is integrated by parts, we obtain

$$\frac{dD^2}{dy} = -(4\pi y)^{-1} \int_0^\infty (v+1)^{-3/2} \sin[2\pi y^2 v]dv. \tag{42}$$

Since $(v+1)^{-3/2}$ is a monotonically decreasing function of v and $\sin[2\pi y^2 v]$ is positive for $0 \leqslant v \leqslant (2y^2)^{-1}$, the integral is always positive for all values of y and dD^2/dy is negative for $y>0$. Thus the distance from $H(y)$ to $(1+i)/4$ steadily decreases. Figure 3 shows the variation of $H(y)$ in the complex plane for positive values of y.

Equation (27) demonstrates that $F(x)$ depends upon $h(y,U) = H(y) + H(U-y)$. Therefore, we can deduce the behavior of $F(x)$ from that of H. Using Eq. (17), we may write

$$|H(y) - (1+i)/4| \leqslant 4/(4\pi y) = 1/\pi y, \tag{43}$$

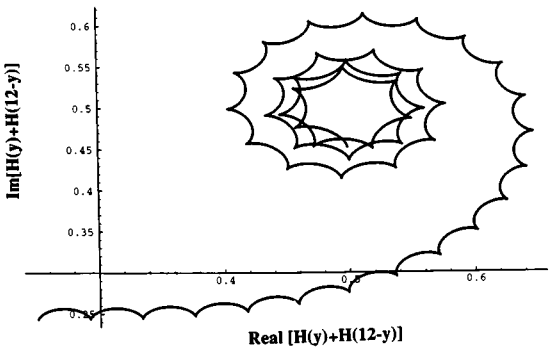

FIG. 4. Plot of $H(y)+H(12-y)$ in the complex plane for real values of y over the range $0\leqslant y\leqslant 2$. As y increases, the sum of $H(y)+H(12-y)$ is seen to approach the limiting value of $(1+i)/2$.

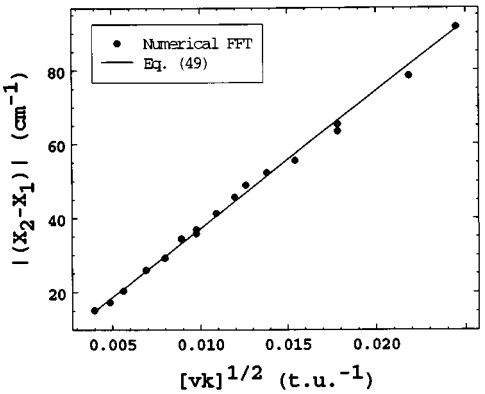

FIG. 5. $|\Delta x^1_{\max}|=|x_{(m=2)}-x_{(m=1)}|$ as defined by Eq. (48) in the text as a function of $(\nu_0 k)^{1/2}=\alpha^{1/2}$. The solid line is the theoretical result from the analytic Fourier transform, Eq. (49). The points are calculated numerically using a FFT method.

where we have taken $p(y)=2\pi y^2$ so that $p'(y)=4\pi y$ which is clearly $\geqslant 4\pi y>0$ for all y. From Eq. (43), it follows that

$$H(U-y)=(1+i)/4+\Theta/[\pi(U-y)], \tag{44}$$

where $|\Theta|\leqslant 1$. Thus $H(U-y)$ makes a small spiral in the complex plane very close to $(1+i)/4$ while $H(y)$ makes a large spiral around $(1+i)/4$. The sum of the two spirals therefore makes a spiral around $(1+i)/2$ which is spiraling closer to the target but has some zigs in it. The result is shown in Fig. 4 for the case $U=12$. The main peaks of $|h(y,U)|^2$ therefore occur at the peaks of $|H(y)|^2$ with smaller maxima occurring between the major peaks. These smaller maxima are clearly seen in Fig. 1(A).

For the system described by Eq. (16), we have

$$y=b/2\alpha^{1/2}=(\nu_0-x)/\{2\alpha^{1/2}\}. \tag{45}$$

The nth extrema for $|H(y)|^2$ occurs at $y=s_n^{1/2}$ so that the corresponding frequency is

$$x_n=\nu_0-2(s_n\alpha)^{1/2}. \tag{46}$$

Since we expect the mth maximum to occur very near $[m-5/8]^{1/2}$, we have

$$x_m\approx\nu_0-2(m-5/8)^{1/2}\alpha^{1/2} \quad \text{for } (m=1,2,3,\ldots). \tag{47}$$

The spacing between successive maxima will therefore be

$$\begin{aligned}\Delta x^m_{\max}&=-2\alpha^{1/2}(s^{1/2}_{2m+1}-s^{1/2}_{2m-1})\\ &\approx-2\alpha^{1/2}[(m+1-5/8)^{1/2}-(m-5/8)^{1/2}].\end{aligned} \tag{48}$$

Equation (48) shows that $\Delta x^m_{\max}$ is independent of the total time for the process T and that it scales with $\alpha^{1/2}$. Since $\alpha=\nu_0 k=|d\nu/dt|$, the above analysis demonstrates that the peak-to-peak spacing is a direct measure of the rate of change of the vibrational frequency of the oscillator.

The largest fine structure spacing will be the easiest to extract accurately. This corresponds to $\Delta x^1_{\max}=x_{(m=2)}-x_{(m=1)}$. The results given above show that

$$\Delta x^1_{\max}=-2\alpha^{1/2}(s^{1/2}_{n=3}-s^{1/2}_{n=1})=-1.13\cdots\alpha^{1/2}. \tag{49}$$

Figure 5 shows a comparison of $|\Delta x^1_{\max}|$ obtained from numerical FFT calculations for different choices of α and the result predicted by Eq. (49). As can be seen, the agreement is good to excellent. Most of the deviations are due to the limited resolution of the numerical transform.

The CFM effect provides the explanation for the observations reported by Noid *et al.*,[3] Smith and Shirts,[4] Dumont and Brumer,[5] and Chang *et al.*[6] Noid *et al.*[3] found that ergodic dynamics leads to broadened spectra containing many smaller peaks. Since the IVR rate in an ergodic system is large, we expect the internal energy present in various modes to vary rapidly. Since the bond potentials are anharmonic, this will lead to a continuous frequency variation that will produce the type of broadening and fine structure seen in Fig. 1. Smith and Shirts[4] noted that ensemble-average spectra do not exhibit the expected ''grassiness'' with increasing energy, but that the spectra of individual trajectories do. In the next section, we will show that this observation is a result of the CFM effect. The diagnostic tests proposed by Chang *et al.*[6] are also a direct consequence of the CFM effect that produces very broad spectral bands each containing a wealth of fine structure. Figures 3(b) and 7(b) of Ref. 6 provide illustrative examples of power spectra in which several bands simultaneously take on the general appearance of those shown in Fig. 1.

Many physical processes are associated with first-order rate laws rather than zero order. If these processes produce a frequency modulation, we would expect an exponential variation of ν_0 rather than the linear decrease in Eq. (13). That is, we expect $f(t)$ to have the form

$$\begin{aligned}f(t)&=r(t)-r_e\\ &=A\,\sin[2\pi\nu_0\,\exp\{-kt\}t] \quad \text{for } 0\leqslant t\leqslant T\\ &=0 \quad \text{otherwise.}\end{aligned} \tag{50}$$

We have carried out numerous numerical experiments to determine the shape of the power spectral band for a ''harmonic'' oscillator described by Eq. (50). Figure 6 shows one result for the case $k=0.0005$ t.u.$^{-1}$ and $\nu_0=2.00$ t.u.$^{-1}$. The qualitative appearance of the power spectrum is similar to those seen in Fig. 1. The band is broadened and the fine

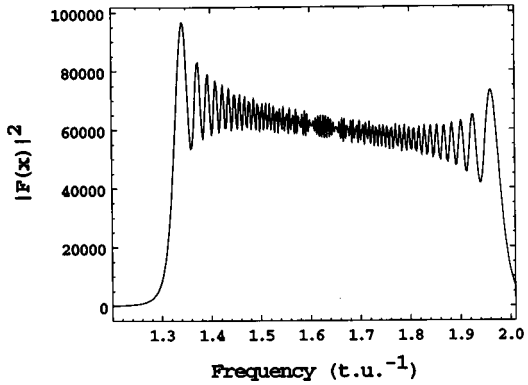

FIG. 6. Power spectrum for the oscillator defined by Eq. (50) in the text with $A=2.0$ Å, $\nu_0=2.0$ t.u.$^{-1}$ and $k=0.0005$ t.u.$^{-1}$ (1 t.u.$=1.018\times10^{-14}$ s). The power spectrum was computed with a fast Fourier transform (FFT) method using 4096 equally spaced values of $r(t)$ calculated using Eq. (50).

structure components exhibit the characteristic spacing variations. However, the high and low frequency Fourier components no longer have equal intensity. Equation (13) gives all frequency domains equal weight, but the exponential variation in Eq. (50) weights the low-frequency components more heavily since the weight is proportional to $|d\nu/dt|^{-1}$.

If it is assumed that we may generalize the analytic result obtained for the oscillator described by Eqs. (12) and (13), we might write

$$\Delta x^m_{\max}=-2(s^{1/2}_{2m+1}-s^{1/2}_{2m-1})|d\nu/dt|^{1/2}=-K|d\nu/dt|^{1/2}, \tag{51}$$

where K is a constant characteristic of the particular type of oscillator being considered. When the oscillator is described by Eq. (50), $|d\nu/dt|=k\nu$. If we also assume that the fine structure spacing is primarily determined by the maximum value of $|d\nu/dt|$, we would expect $\Delta x^1_{\max}$ to be given by

$$\Delta x^1_{\max}=-K(k\nu_0)^{1/2}. \tag{52}$$

Figure 7 demonstrates the extent to which Eq. (52) holds for an exponentially varying frequency. The level of agreement between the spacing obtained from the FFT of Eq. (50) for

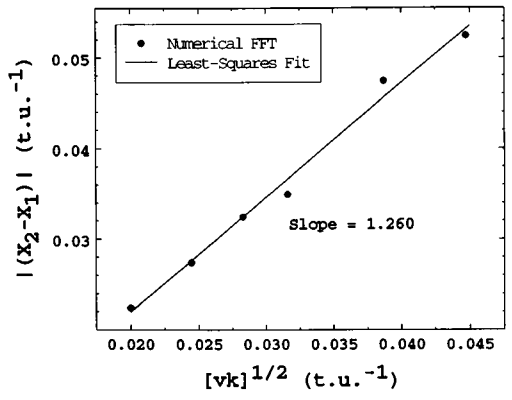

FIG. 7. $|\Delta x^1_{\max}|=|x_{(m=2)}-x_{(m=1)}|$ as a function of $(\nu_0 k)^{1/2}$ for the oscillator defined by Eq. (50) in the text with $A=2.0$ Å, $\nu_0=2.0$ t.u.$^{-1}$ and $k=0.0005$ t.u.$^{-1}$ (1 t.u.$=1.018\times10^{-14}$ s).

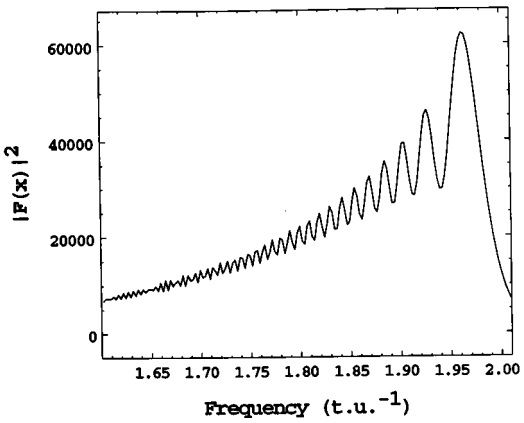

FIG. 8. Power spectrum for the oscillator defined by Eq. (53) in the text with $A=2.0$ Å, $\nu_0=2.0$ t.u.$^{-1}$, $k_2=0.001$ t.u.$^{-1}$, and $k_1=0.0005$ t.u.$^{-1}$ (1 t.u.$=1.018\times10^{-14}$ s). The power spectrum was computed with a fast Fourier transform (FFT) method using 4096 equally spaced values of $r(t)$ calculated using Eq. (53).

different values of k and Eq. (52) is generally good. The slope of the least-squares fit to the data gives $K=1.26$, which is slightly larger than the theoretical result for the linear variation of ν_0 given in Eq. (49).

When the CFM effect is the result of IVR, we expect an attenuation of the oscillator's amplitude as well as a variation of its frequency. A simple harmonic model reflecting this expectation is

$$f(t)=r(t)-r_e=A\ \exp\{-k_2t\}\sin[2\pi\nu_0\ \exp\{-k_1t\}t]$$
$$\text{for } 0\leqslant t\leqslant T$$
$$=0 \quad \text{otherwise.} \tag{53}$$

The power spectrum band for the oscillator described by Eq. (53) may lose its low-frequency components due to the amplitude attenuation. Figure 8 shows a typical example.

III. CFM EFFECTS FOR A MORSE OSCILLATOR

For any anharmonic potential, the vibration frequency will be a function of the oscillator energy. As a result, energy transfer to or from the oscillator will produce a CFM effect and a complex power spectrum for a large molecule.[6] To simulate internal energy transfer for an anharmonic potential, we consider a Morse oscillator whose kinetic energy decays exponentially with time. That is, we write the Hamiltonian as

$$H=T\ \exp\{-2kt\}+V(r), \tag{54}$$

where $V(r)$ is given by Eq. (10). Such an oscillator will exhibit both a CFM effect and an attenuation of amplitude. Fourier transforms of $r(t)$ for two specific cases are shown in Figs. 9(A) and 9(B). The effect of the amplitude attenuation is obvious in the plots. It is also clear that the fine structure spacing is increasing with increasing values of k in Eq. (54).

A useful expression for the fine structure spacing of a Morse oscillator can be obtained from Eq. (51),

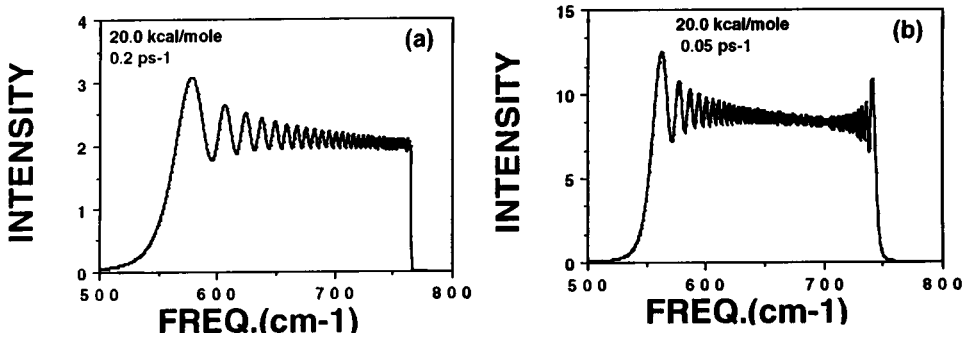

FIG. 9. Power spectra for a Morse oscillator whose Hamiltonian is given by Eq. (54) with $D=40.7985$ kcal/mol, $\beta=2.1364$ Å^{-1}, $r_e=1.3776$ Å. k and the initial energy E_0 as given in the figures. The reduced oscillator mass is 7.47 amu.

$$\Delta x^1_{\max} = -K|d\nu/dt|^{1/2} = -K|(d\nu/dE)(dE/dt)|^{1/2}. \tag{55}$$

From Eq. (11), we obtain

$$\frac{d\nu}{dE} = -(\beta/4\pi)[2/\mu]^{1/2}[D-E]^{-1/2}. \tag{56}$$

Since many IVR processes are first order and Eq. (54) suggests a first-order energy transfer rate, we have for the total energy

$$\frac{dE}{dt} = -kE. \tag{57}$$

Combination of Eqs. (55)–(57) gives

$$\Delta x^1_{\max} = -K\{(kE\beta/4\pi)[2/\{\mu(D-E)\}]^{1/2}\}^{1/2}. \tag{58}$$

If we again assume that the fine structure spacing is primarily determined by the maximum value of $|d\nu/dt|$, E may be replaced with E_0, where E_0 is the initial energy of the oscillator.

Equation (58) provides the explanation of the observation made by Smith and Shirts[4] that ensemble-averaged power spectra do not exhibit the grassiness seen in the spectra of individual trajectories. The IVR rate constants associated with individual trajectories differ. Consequently, $\Delta x^1_{\max}$ will vary from trajectory to trajectory. As a result, destructive interference between the spectral lines will tend to remove the grassiness from ensemble-average power spectra.

Table I gives a comparison of $|\Delta x^1_{\max}|$ values obtained by taking the Fourier transform of $r(t)$ computed using Eq. (54) with those predicted by Eq. (58) with E set equal to E_0. The table reports results for a wide range of the variables: 1 kcal/mol$\leqslant E_0 \leqslant$40.0 kcal/mol, 40.8 kcal/mol$\leqslant D \leqslant$115.0 kcal/mol, 0.05 ps$^{-1}\leqslant k \leqslant$1.0 ps^{-1}, 2.1364 Å$^{-1}\leqslant\beta\leqslant$4.2728 Å^{-1}, 0.95 amu$\leqslant\mu\leqslant$7.47 amu. A least-squares fit of K to the results of 125 sets of computations in these ranges gives $K=2/3$. With this value for K, $|\Delta x^1_{\max}|$ varies from 2.7 to 144.5 cm^{-1}, where 1 t.u.$^{-1}$ corresponds to 3278 cm^{-1}. The ratio of the Fourier transform result to that given by Eq. (58) varies from 0.51 to 1.98 with an average value equal to 0.99. The distribution has a standard deviation of 0.21. Consequently, we might expect that the use of Eq. (58) to extract energy transfer rate coefficients from the spacing of the power spectrum fine structure components would lead to errors on the order of $\pm$25%.

IV. AN EXPERIMENTAL EXAMPLE OF THE CFM EFFECT

Since the CFM effect is dependent only upon the existence of a time-varying resonant frequency, any system satisfying this condition should, in principle, exhibit spectral line shapes similar to those seen in Figs. 1, 6, 8, and 9, provided that the frequency variation occurs on a time scale comparable to the data acquisition time. These conditions suggest that an obvious place to look for CFM effects is nuclear magnetic resonance (NMR) spectroscopy.

In a pulsed NMR experiment, the system is placed in a strong, uniform and constant magnetic field. The interaction of the field, $\mathbf{B_0}$, with the nuclear magnetic moment splits the otherwise degenerate nuclear spin states. Transitions between these states are induced by the frequency components of the electromagnetic pulse whose energy matches the splitting between the states. Fourier analysis of the transmitted pulse permits a determination of the frequency components that have been absorbed. Since the state splitting is proportional to the externally applied field, care must be exercised to ensure that $\mathbf{B_0}$ remains a known constant throughout the experiment. This is generally accomplished by means of an electronic field/frequency lock.

The foregoing discussion describes the normal procedure used in taking an NMR spectrum. For example, consider a mixture of slightly soluble H_2O in $HCCl_3$. Since the two water protons are equivalent, a standard NMR ^{1}H spectrum would be expected to exhibit two sharp single absorption lines separated by the internal chemical shift produced by the different electronic environments about the H_2O and $HCCl_3$ protons. If, however, $\mathbf{B_0}$ varied during the experiment, the splitting between the spin states would change continuously. As a result, the resonant frequencies would exhibit a CFM effect.

We have conducted such an experiment on a sample of neat $DCCl_3$ containing a small amount of H_2O and $HCCl_3$. The data were taken on a Bruker WP-200 spectrometer via a

TABLE I. Comparison of $\Delta x^1_{\max}$ values obtained from the FFT of $r(t)$ calculated using Eq. (54) with those predicted by Eq. (58) with E replaced with E_0 and $K=2/3$.

Energy (kcal/mol)	k (ps^{-1})	$\Delta x^1_{\max}$ (cm^{-1}) FFT	Eq. (58)	Energy (kcal/mol)	k (ps^{-1})	$\Delta x^1_{\max}$ (cm^{-1}) FFT	Eq. (58)
$D=115.0195$ kcal/mol, $\beta=2.6228$ Å^{-1} $\mu=7.47$ amu				$D=78.8310$ kcal/mol, $\beta=2.4459$ Å^{-1} $\mu=0.948$ amu			
40.0	1.00	69.55	70.98	40.0	1.00	144.54	135.38
40.0	0.50	50.45	50.19	40.0	0.50	109.09	95.73
40.0	0.20	34.09	31.74	40.0	0.20	80.45	60.55
40.0	0.05	10.91	15.87	40.0	0.05	60.00	30.27
20.0	1.00	43.64	47.31	20.0	1.00	90.00	86.29
20.0	0.50	32.73	33.45	20.0	0.50	68.18	61.01
20.0	0.20	21.82	21.16	20.0	0.20	49.09	38.59
20.0	0.05	10.91	10.58	20.0	0.05	34.09	19.29
10.0	1.00	25.91	32.63	10.0	1.00	57.27	58.67
10.0	0.50	20.45	23.07	10.0	0.50	45.00	41.48
10.0	0.20	15.00	14.59	10.0	0.20	31.36	26.24
10.0	0.05	8.18	7.30	10.0	0.05	21.82	13.12
5.0	0.50	13.64	16.13	5.0	1.00	36.82	40.76
5.0	0.20	9.54	10.20	5.0	0.50	28.64	28.82
5.0	0.05	5.46	5.10	5.0	0.20	20.45	18.23
				5.0	0.05	13.64	9.11
2.0	0.20	4.09	6.41				
2.0	0.05	4.09	3.20	2.0	1.00	13.64	25.52
				2.0	0.50	16.36	18.05
				2.0	0.20	10.91	11.41
				2.0	0.05	8.18	5.71
				1.0	1.00	10.91	17.99
				1.0	0.50	6.82	12.72
				1.0	0.20	8.18	8.05
				1.0	0.05	5.45	4.02
$D=40.7985$ kcal/mol, $\beta=2.1364$ Å^{-1} $\mu=7.47$ amu				$D=40.7985$ kcal/mol, $\beta=3.2046$ Å^{-1} $\mu=7.47$ amu			
20.0	1.00	61.36	62.43	20.0	1.00	72.27	76.45
20.0	0.50	43.64	44.14	20.0	0.50	54.55	54.06
20.0	0.20	27.96	27.92	20.0	0.20	34.09	34.19
20.0	0.05	15.00	13.96	20.0	0.05	19.09	17.10
15.0	1.00	47.73	51.23	15.0	1.00	60.00	62.74
15.0	0.50	35.46	36.22	15.0	0.50	43.64	44.36
15.0	0.20	23.18	22.91	15.0	0.20	28.64	28.06
15.0	0.05	12.27	11.46	15.0	0.05	16.36	14.03
10.0	1.00	34.09	40.02	10.0	1.00	43.64	49.01
10.0	0.50	26.59	28.30	10.0	0.50	34.09	34.65
10.0	0.20	18.41	17.90	10.0	0.20	21.82	21.92
10.0	0.05	9.55	8.95	10.0	0.05	12.27	10.96
5.0	1.00	17.73	27.25	5.0	1.00	25.91	33.37
5.0	0.50	16.36	19.27	5.0	0.50	21.82	23.60
5.0	0.20	12.27	12.19	5.0	0.20	15.00	14.93
5.0	0.05	6.14	6.09	5.0	0.05	8.18	7.46
2.0	1.00	10.23	16.89	2.0	0.50	10.91	14.63
2.0	0.20	6.14	7.55	2.0	0.20	8.18	9.25
2.0	0.05	3.41	3.78	2.0	0.05	5.46	4.63
1.0	0.50	5.46	8.39	1.0	0.20	5.46	6.50
1.0	0.20	2.73	5.31	1.0	0.05	2.73	3.25
1.0	0.05	2.73	2.65				

TABLE I. *(Continued).*

Energy (kcal/mol)	k (ps^{-1})	$\Delta x^1_{\max}$ (cm^{-1}) FFT	Eq. (58)	Energy (kcal/mol)	k (ps^{-1})	$\Delta x^1_{\max}$ (cm^{-1}) FFT	Eq. (58)
$D=40.7985$ kcal/mol, $\beta=4.2728$ Å^{-1} $\mu=7.47$ amu				$D=60.000$ kcal/mol, $\beta=2.1364$ Å^{-1} $\mu=7.47$ amu			
20.0	1.00	84.55	88.28	20.0	1.00	49.09	53.01
20.0	0.50	62.73	62.42	20.0	0.50	36.82	37.48
20.0	0.20	40.91	39.48	20.0	0.20	24.55	23.71
20.0	0.05	21.82	19.74	20.0	0.05	12.27	11.85
15.0	1.00	69.55	72.44	15.0	1.00	39.55	44.57
15.0	0.50	53.18	51.23	15.0	0.50	31.36	31.52
15.0	0.20	34.09	32.40	15.0	0.20	20.45	19.93
15.0	0.05	17.73	16.20	15.0	0.05	10.91	9.97
10.0	1.00	53.18	56.59	10.0	1.00	27.27	35.45
10.0	0.50	40.91	40.01	10.0	0.50	23.18	25.07
10.0	0.20	27.27	25.31	10.0	0.20	16.36	15.85
10.0	0.05	13.64	12.65	10.0	0.05	8.18	7.93
5.0	1.00	32.73	38.54	5.0	0.50	13.64	17.31
5.0	0.50	27.27	27.25	5.0	0.20	10.91	10.95
5.0	0.20	17.73	17.23	5.0	0.05	5.45	5.47
5.0	0.05	9.54	8.62				
				2.0	0.20	5.45	6.83
2.0	0.50	13.64	16.89	2.0	1.00	9.55	15.28
2.0	0.20	10.91	10.68	2.0	0.05	4.09	3.42
2.0	0.05	5.46	5.34				
				1.0	0.50	4.09	7.61
1.0	1.00	10.91	16.78				
1.0	0.20	6.82	7.51				
1.0	0.05	4.09	3.75				

single scan with the field/frequency lock off but the field still scanning. The resulting FID (free induction decay) signal and power spectrum are shown in Fig. 10. The bands labeled A_2 and A_3 are the FID signals obtained from the $HCCl_3$ and H_2O protons, respectively. Their qualitative appearance bears a very close resemblance to $r(t)$ obtained from Eq. (53). The signal labeled A_1 is an electronic transient. If the field is locked, the A_2 and A_3 bands each appear as a single sharp line very similar in appearance to the A_1 band. The bands in the power spectrum corresponding to the FID bands are labeled B_1, B_2, and B_3, respectively. Figure 10 also shows an expanded view of A_2 and B_2. The resemblance of the B_2 band to the band shape shown in Fig. 6 is remarkable. In both cases, there is an attenuation of the importance of the frequency components at one end of the pattern. Each power spectrum exhibits the characteristic fine structure with decreasing peak-to-peak spacings. The B_3 band shows many points of similarity to the power spectrum seen in Fig. 8. Clearly, a CFM effect is present. We could determine the rate at which $\mathbf{B_0}$ is being varied from the fine structure spacing $\Delta x^1_{\max}$.

In a standard NMR spectrum, the normal T_2 decay during acquisition results in the FID being attenuated at longer times—the signal decays with time. This is seen in both the peaks labeled A_2 and A_3 in Fig. 10. The relaxation time of A_2 is sufficiently long that the FID has not completely de-

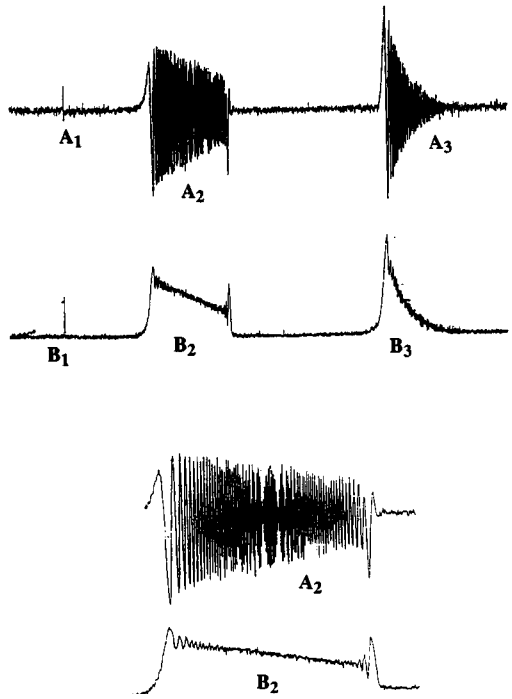

FIG. 10. Fourier transform NMR signals illustrating the CFM effect produced by varying the main B field during the experiment. Trace labeled (A) is the FID signal. Trace (B) is the corresponding power spectrum. Top: Results obtained from $HCCl_3$ (A_2) and water (A_3) in $DCCl_3$. The signal labeled A_1 is an electronic transient. Bottom: An expanded view of the $HCCl_3$ signal.

cayed at the end of the acquisition. The net result is the fine structure at the right of end of B_2 and its absence in B_3.

As an added note of interest, it is of some importance to note that the electronic transient, A_1, is unaltered by the variation of $\mathbf{B_0}$. Since its origin is electronic rather than a splitting of the nuclear spin states, it exhibits no CFM effect. This observation suggests a method for identification of such transients in a complex NMR spectrum. One simply removes the field lock and takes an NMR spectrum with $\mathbf{B_0}$ varying. All the NMR lines will broaden and split, but the electronic transients will be unaffected. Once identified, they may be safely subtracted from the NMR spectrum.

V. APPLICATIONS: ENERGY TRANSFER IN A MATRIX AND IVR

As a first test, we have used the CFM effect to extract the rate of energy transfer from a diatomic molecule to a surrounding matrix cage of argon atoms at 12 K. This system is sufficiently simple to permit a straightforward interpretation of the computed power spectrum. It also allows the energy transfer rate to be determined by standard methods[15] unrelated to the CFM effect. This provides a benchmark against which the CFM results may be tested.

The matrix model used in the calculations is a face-centered cubic argon lattice containing 125 unit cells (666 atoms) in a $5\times5\times5$ arrangement along the principal axes of the crystal with the center of mass at the origin. The center of mass of the diatomic molecule is placed at the origin and the molecule is randomly oriented relative to the lattice. The

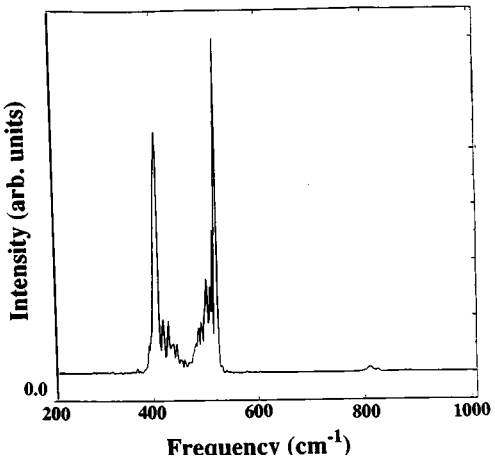

FIG. 11. Power spectrum of a diatomic Morse oscillator matrix isolated in a face-centered cubic argon lattice at 12 K. Potential parameters and model description are given in the text.

matrix is then allowed to relax around the molecule to its nearest local potential minimum by execution of a damped trajectory[15] of the matrix atoms. The diatomic bond potential is described by a Morse potential, Eq. (10), with $D=2.514$ eV, $\beta=2.002$ Å^{-1}, $r_e=1.988$ Å, and $\mu=17.4844$ amu. The potential energy of the matrix is taken to be a sum of pairwise Morse potentials whose parameters are taken from the literature.[2(b)] The molecule-matrix interaction potential is also written as a sum of pairwise Morse terms with parameters obtained using standard combining rules.[16] Interactions with the matrix bulk are simulated using the velocity reset procedure developed by Riley, Coltrin, and Diestler.[17] Reference 15 describes the procedures in more complete detail.

To investigate energy transfer rates from molecular vibration to the phonon modes of the lattice, the diatomic molecule is given an initial vibrational energy $E_0=1.5$ eV and zero rotational energy. The initial vibrational phase is selected randomly. Energy loss rate coefficients, k_{traj}, are obtained from the slope of a decay plot of $\ln(E)$ versus time for an ensemble of trajectories. Power spectra for the diatomic are computed using an FFT method with 2 cm^{-1} resolution. The corresponding energy loss coefficient, k, is extracted from the power spectrum of individual trajectories using Eq. (58). These rate coefficients are then averaged to obtain the ensemble result which may be compared directly with k_{traj}.

Figure 11 shows a typical power spectrum of the diatomic Morse oscillator for one trajectory. The CFM effect produced by energy transfer to the lattice is obvious. The general pattern of the fine structure is more complex than that seen in the model spectra shown in Figs. 1, 6, 8, and 9. This is due to the more complex potential of the matrix system and to the fact that energy flow to the lattice is not rigorously a first-order process. If we extract $\Delta x^1_{\max}$ from Fig. 11 and use Eq. (58) with $K=2/3$, we obtain $k=(4.6\pm1.8)\times10^{-4}$ t.u.$^{-1}$, where the error limits are computed from the uncertainty in the spectral resolution. An ensemble average of 20 trajectories yields $\langle k\rangle=(3.3\pm1.6)\times10^{-4}$ t.u.$^{-1}$. The slope of the energy decay

plot for these 20 trajectories gives $k_{\text{traj}}=(4.6\pm0.25)\times10^{-4}$ t.u.$^{-1}$. The agreement between $\langle k\rangle$ and k_{traj} is not surprising since the error expected from the use of Eq. (58), $\pm25\%$, is less than the uncertainty due to the limited spectral resolution.

We have also utilized the CFM effect to compute IVR rate coefficients for *cis*-HONO. The potential surface developed by Chambers and Thompson[18] is used in all calculations. The IVR rate subsequent to excitation of the N═O or the O–H local mode is investigated by computation of an ensemble-averaged energy decay plot and by averaging individual rate coefficients obtained from the fine structure spacings using Eq. (58). Since the average IVR rates depend on whether or not *cis*→*trans* isomerization occurs, the averages are performed only over those trajectories which do not isomerize.

Energy transfer out of a local N═O stretching mode was studied by the computation of a batch of 100 trajectories. The initial HONO internal states were prepared by random insertion of zero-point energy into each of the six vibrational modes with the rotational energy set to zero. Four additional quanta of vibrational energy were then partitioned into the normal mode corresponding to the N═O stretch. Phase averaging was incorporated by a random selection of phase for each normal mode. Subsequently, the vibrational energy was scaled to a final value of 31.6 kcal/mol. At this stage, the energy in the local N═O stretching mode was 17.6 kcal/mol. Each trajectory was propagated for 12.82 ps or until *cis*→*trans* isomerization occurred. A total of 47 trajectories did not isomerize.

Figure 12(A) gives a typical power spectrum of the N═O stretching coordinate. The average separation between the first two fine structure peaks is 5.2 cm^{-1} which corresponds to a frequency of 0.001 59 t.u.$^{-1}$ or 0.156 ps^{-1}. This spacing is marked by arrows in Fig. 12(A). The N═O bond potential is a Morse function with $D=115.0195$ kcal/mol and $\beta=2.6228$ Å^{-1}. The use of these values in Eq. (58) with $K=2/3$ gives an ensemble-averaged energy transfer rate coefficient $k=0.014$ ps^{-1}. The energy decay plot obtained from the 47 trajectories that did not isomerize is shown in Fig. 12(B). The slope of the least-squares line gives $k=0.011$ ps^{-1}. The difference between the results of the two methods corresponds to 27% of the result obtained from the decay plot.

Similar studies of IVR out of the local O–H stretching coordinate were also executed. Energy transfer rate coefficients were computed from the results of 511 trajectories of which 218 did not isomerize. In each trajectory, the total energy in HONO was scaled to 32.6 kcal/mol with 22.0 kcal/mol partitioned into the local O–H stretching mode. The Morse parameters for the O–H bond are $D=78.8310$ kcal/mol and $\beta=2.4459$ Å^{-1}. The ensembled-averaged IVR rate coefficient obtained from the fine structure spacing using Eq. (58) is 0.040 ps^{-1}. The slope of the energy decay plot yields a value of 0.036 ps^{-1}.

The above results demonstrate that power spectrum line shapes can be effectively used as probes of IVR rates. Comparison of rates extracted from line shapes and the slopes of

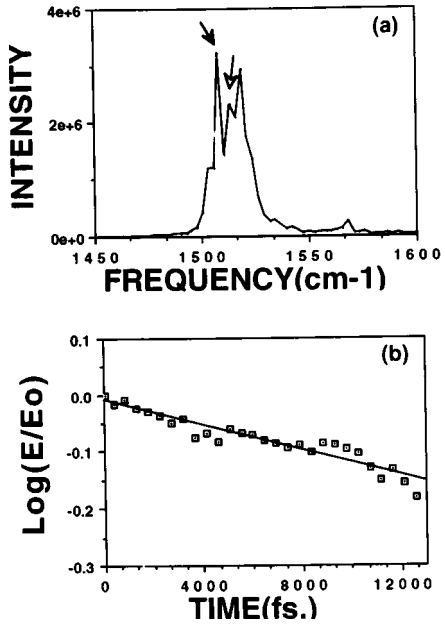

FIG. 12. (A) Power spectrum obtained from a fast Fourier transform of the time dependence of the N═O bond distance in *cis*-HONO. The total *cis*-HONO internal energy is 31.6 kcal/mol of which 17.6 kcal/mol is initially partitioned into the local N═O stretching coordinate. The arrows indicate the two fine structure peaks considered in the calculation. (b) Ensemble-averaged energy decay plot for the local N═O mode energy. The initial local N═O mode energy is 17.6 kcal/mol. The total *cis*-HONO internal energy in all trajectories is 31.6 kcal/mol.

energy decay curves agree to within 27% for N═O relaxation and 11% for energy transfer from the O–H stretching mode. These differences result from a combination of the approximations made to obtain Eq. (58), the limited spectral resolution and the statistical errors present in the decay plots.

VI. APPLICATION: IVR IN SMALL MOLECULES

Equations (57) and (58) will usually provide a sufficiently accurate description of energy decay from a local mode in systems possessing a heat bath or for large molecules containing many internal modes. In such systems, entropy effects minimize the back transfer of energy to the decaying mode. The result is a near exponential decay of energy from the relaxing mode as predicted by Eq. (57). However, this type of relaxation is not expected for small, isolated molecules containing only two or three vibrational modes.

The internal energy in two or three mode systems generally exhibits a complex, oscillatory behavior. As the trajectory explores phase space, the energy and instantaneous frequencies evolve in a complex pattern that depends upon the intramolecular potential and the initial conditions of the trajectory. Under these conditions, Eqs. (57) and (58) will not provide a useful description of the energy transfer rates. Nevertheless, we still expect to observe a CFM effect with the band spacings related to the instantaneous frequency variations by Eq. (55). This observation suggests that the present methods can be effectively combined with the technique of local frequency analysis developed by Martens, Davis, and

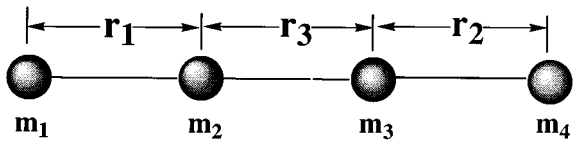

FIG. 13. Four-atom, collinear model and definition of coordinates.

Ezra[19] and by McDonald and Marcus[20] and Marcus, Hase and Swamy[21] in which fast Fourier transforms are performed over short sequential segments of a long trajectory. These transforms provide the temporal variation of the power spectrum band spacings which can then be directly related to the instantaneous energy transfer rates using Eq. (55).

As a simple illustration, we have applied these methods to the analysis of energy transfer in the simple four-atom, three-mode collinear system shown in Fig. 13. The Hamiltonian for this system is taken to be

$$H=0.5\sum_{i=1}^{4} P_i^2/m_i+V_1(r_1)+V_2(r_2)+V_3(r_3), \tag{59}$$

where $V(r)$ is the Morse potential given by Eq. (10). The potential parameters and masses are given in Table II. In effect, $V_3(r_3)$ functions as a coupling potential between two local stretching modes. If D_3 is set to zero, the system reduces to two, independent Morse oscillators with no energy transfer. We may therefore conveniently discuss the energy flow in terms of two local mode energies, $E1$ and $E2$, where we define

$$E2=0.5[P_4^2/m_4+P_3^2/m_3]+V_2(r_2) \tag{60}$$

with a similar definition for $E1$.

The energy transfer and power spectrum evolution have been examined for a single trajectory in which the initial state has $P_i=0$ for all i, $V_1(r_1)=V_3(r_3)=0$ and $V_2(r_2)=2.5$ eV. Hamilton's equations of motion were integrated for a period of 2000 t.u. (1 t.u.$=0.010\,19$ ps). The temporal variation of the power spectra of r_2 was computed using a fast Fourier transform of a sliding window of 102.2 t.u. (1.04 ps) that was moved along the trajectory in increments of 10 t.u. (0.1019 ps).

Figure 14 shows the variation of $E2$. For the first 1680 t.u. (17.12 ps), $E2$ oscillates rapidly about a mean value of about 2.3 eV with very little net energy transfer out of the mode. Around 1600 t.u. (16.30 ps), the kinetic coupling has increased sufficiently to facilitate energy transfer to mode $E1$. At 1700 t.u. (17.32 ps) and beyond, we observe the large amplitude, complex oscillations of the internal energy that are frequently characteristic of small molecules.

TABLE II. Potential parameters and masses for the four-atom, collinear modelillustrated in Fig. 13. Masses: $m_1=m_2=m_3=m_4=12.0$ amu.

Parameter	Mode 1	Mode 2	Mode 3
D	3.925 eV	3.925 eV	1.000 eV
r_e	1.570 Å	1.570 Å	1.570 Å
β	1.6864 Å^{-1}	1.810 Å^{-1}	1.6864 Å^{-1}

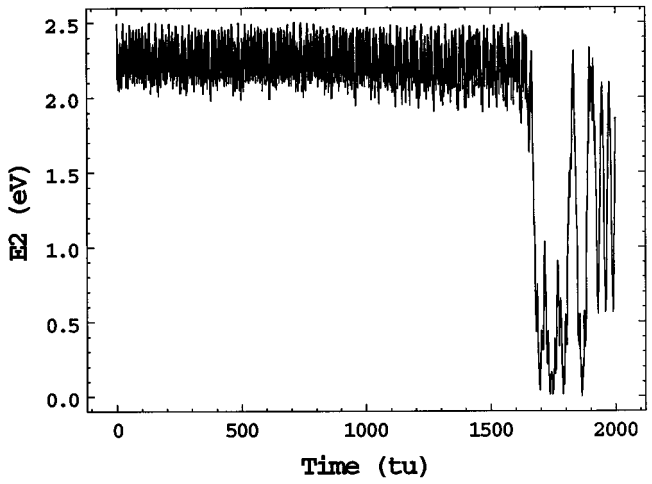

FIG. 14. Temporal variation of the local mode energy, $E2$, defined by Eq. (60) for the four-atom model shown in Fig. 13 with initial conditions as described in the text. 1 time unit (t.u.) is 0.010 19 ps.

Figures 15(A)–15(D) show computed power spectra for the coordinate r_2 obtained with the sliding window spanning the time range shown in the figures. Figure 14(A) shows that the power spectrum of r_2 over the range 1019.6–1121.8 t.u. is a single band centered at 0.225 t.u.$^{-1}$ (737 cm^{-1}). There is no CFM splitting since there is effectively no net energy transfer from the mode during this period of time. Figure 15(B) shows the power spectrum over the range 1638.6–1740.8 t.u. during which $E2$ varies from about 2.4 eV to nearly zero. The CFM splitting of the power spectrum induced by this energy transfer is obvious. Figures 15(C) and 15(D) illustrate the type of changes one sees in the power spectrum as the system evolves.

Figures 16(A) and 16(B) illustrate how the temporal variations of the band spacings resulting from the CFM effect may be used as a probe of the instantaneous energy transfer rates. Figure 16(A) shows $E2$ over the time range 1700 to 1820 t.u. Figure 16(B) gives the computed values of $\Delta X^1_{\max}$ over this same range. In this figure, the calculated band spacing, $\Delta X^1_{\max}$, is plotted as a function of the time corresponding to the leading edge of the temporal window across which the FFT is computed. Equation (55) indicates that we expect $\Delta X^1_{\max}$ to vary with $[dE/dt]^{1/2}$. Consequently, we expect to observe large band spacings over time intervals during which $E2$ is either increasing or decreasing rapidly and small band spacings in ranges where $E2$ remains relatively constant. A straightforward comparison of Figs. 16(A) and 16(B) shows that this correspondence is clearly present. This is particularly true if the accuracy limits due to spectral resolution (± 0.01 t.u.$^{-1}$) and the fact that the method effectively averages $\Delta X^1_{\max}$ over the spectral window are taken into account.

Obviously, the CFM method is not as well suited to the analysis of energy transfer in small systems as is the case for large molecules or systems with large heat baths. Neverthe-

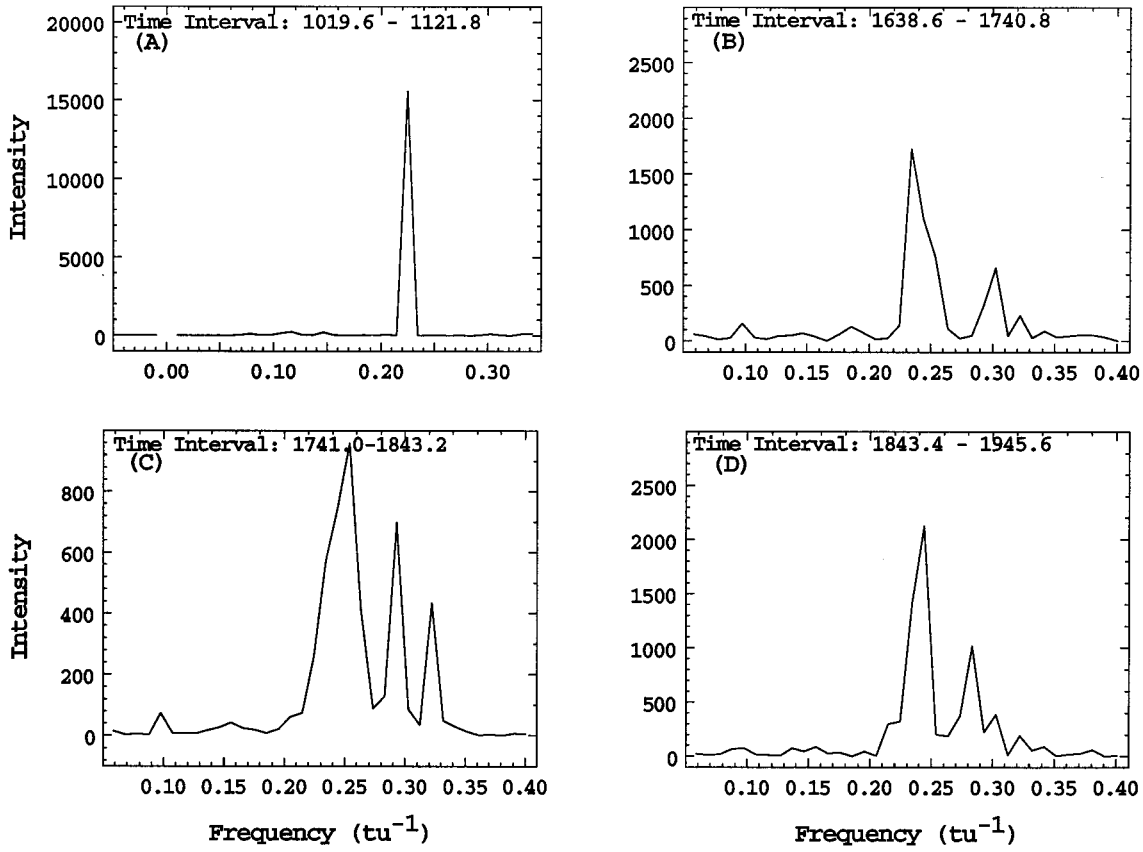

FIG. 15. Power spectra of the $E2$ coordinate r_2 defined in Fig. 13 for the trajectory whose initial conditions are defined in the text. 1 time unit (t.u.) is 0.010 19 ps. (A) Spectral window is 1019.6 to 1121.8 t.u. (B) Spectral window is 1638.6 to 1740.8 t.u. (C) Spectral window is 1741.0 to 1843.2 t.u. (D) Spectral window is 1843.4 to 1945.6 t.u.

less, useful information can still be obtained by examination of the CFM splittings computed using local frequency analysis.[19–21] There is one caveat associated with the use of local frequency analysis that should be considered. The spectral window used to define the instantaneous power spectrum must be long enough to yield sufficient spectral resolution but short enough to ensure that the important dynamic events occur on a time scale longer than the window length. If the IVR rates are extremely large, it may not be possible to simultaneously satisfy both of these conditions.

VII. SUMMARY

We have shown that a continuous frequency modulation (CFM) of an oscillator produces a broadening of the corresponding power spectrum band and the appearance of a wealth of fine structure components. The characteristic fine structure pattern is one of decreasing amplitude and spacing. The CFM effect has been investigated for a series of model oscillators that include harmonic systems with linear and exponential variation of the frequency without amplitude damping, a harmonic system with exponential damping of both the resonant frequency and the amplitude, and a Morse oscillator whose kinetic energy is being exponentially damped.

We have derived an analytic expression for the power spectrum of a harmonic oscillator whose resonant frequency is varying linearly with time. Excellent correspondence between the analytic transform and the numerically computed power spectrum is demonstrated. Analysis of the CFM fine structure using the analytic transform shows that the fine structure peak-to-peak spacing scales with the square root of the absolute value of the modulation rate and is independent of the integration time. We suggest that the CFM effect is the fundamental explanation of several previous empirical observations[3–6] concerning power spectra. The CFM effect for a harmonic system with an exponentially modulated frequency is found to be similar to that obtained for linear modulation. The peak-to-peak fine structure spacing scales approximately with the square root of the absolute value of the modulation rate. However, the proportionality constant is slightly larger than that obtained for linear modulation. Exponential damping of the oscillator amplitude is found to produce a significant decrease in many of the power spectrum bands.

By using a Morse oscillator as a representative system, we have shown that inter- or intramolecular energy transfer can be expected to produce a CFM effect. We have developed an analytic expression relating the peak-to-peak fine structure spacing to the Morse potential parameters, the ini-

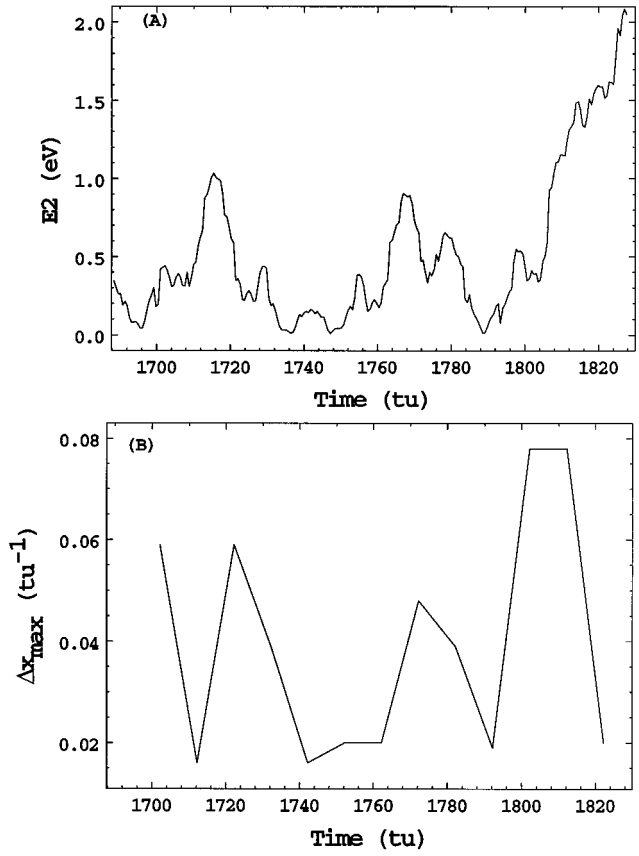

FIG. 16. Comparison of CFM band splitting, $\Delta X^1_{\max}$, with the energy transfer rates to or from local mode $E2$. (A) Temporal variation of the local mode energy, $E2$, defined by Eq. (60) for the four-atom model shown in Fig. 13 with initial conditions as described in the text. 1 time unit (t.u.) is 0.010 19 ps. (B) $\Delta X^1_{\max}$ computed from the FFT of a sliding spectral window of 102.2 t.u. (1.04 ps) that is moved along the trajectory in increments of 10 t.u. (0.1019 ps).

tial internal oscillator energy and an assumed first-order energy transfer rate coefficient. This expression is obtained by assuming that the analytic result for a harmonic oscillator with a linear modulation is transferable to the anharmonic case. Numerical calculations suggest that the result has an expected error of about $\pm 25\%$.

An experimental example of the CFM effect is presented using a modified NMR measurement. By removing the field/frequency lock of the spectrometer and varying $\mathbf{B_0}$ during the experiment, a continuous variation in the resonant NMR frequency is produced. NMR spectra of H_2O and $HCCl_3$ taken under these conditions are found to exhibit the characteristic CFM pattern. It is also shown that this method can provide a useful tool for identifying electronic transients in an NMR spectrum.

We have used the CFM effect to calculate the energy transfer rate coefficient for a diatomic molecule isolated in a cryogenic Ar matrix at 12 K. A 666-atom model of a face-centered cubic argon matrix is used with pairwise Morse potentials. The interaction between the diatomic and the lattice is also represented by a pairwise sum. The diatomic potential is a Morse function. Energy transfer rate coefficients for each trajectory are extracted from the fine structure spacing of the numerically computed power spectrum of $r(t)$. These individual rate coefficients are averaged over an ensemble of 20 trajectories for comparison with the ensemble average obtained from the slope of a standard energy decay plot. The two results differ by about 28%, which is well within the combined error limits of the two calculations.

Similar results are obtained when power spectrum line shapes are used to extract IVR rate coefficients for energy transfer out of the N═O and O–H bonds in *cis*-HONO. In this case, the ensemble-averaged rate coefficients obtained from line shapes agreed with those calculated from the slopes of energy decay plots to within 27% and 11% for the N═O and O–H stretching modes, respectively. We conclude that line shape analysis can be effectively used as a probe of energy transfer rates in systems undergoing continuous frequency modulation.

It is noted that although IVR in small molecules is generally not exponential, CFM methods may be combined with local frequency analysis to obtain a measure of the instantaneous energy transfer rates from the CFM band spacings provided the time scale of the important dynamic events is not short compared to the spectral window that must be employed to compute the power spectra. Application of this combined procedure to a simple, four-atom collinear system demonstrates that there is good correlation between the local energy transfer rates inferred from the computed band spacings and those obtained by direct computation of the temporal variation of the local mode energy.

ACKNOWLEDGMENTS

We are pleased to acknowledge financial support from the National Science Foundation on Grants No. CHE-9211925 and DMS 9500857 and from the Air Force Office of Scientific Research Grant No. F49620-92-J-0011. P.M.A. thanks Vikram University, Ujjain, India, for granting him leave to pursue this research and R.D.K. thanks Gordon College for granting him a sabbatical leave. P.M.A. also wishes to thank Professor Ramesh Sharda and his family for their hospitality during the course of this work.

[1] Several survey articles are available. For example, see (a) Barbara J. Garrison, K. B. S. Prasad, and Deepak Srivastava, Chem. Rev. (to be published); (b) L. M. Raff and D. L. Thompson, in *Theory of Chemical Reaction Dynamics*, edited by M. Baer (CRC, Boca Raton, FL, 1985), Vol. III, p. 1.

[2] For example, see (a) E. J. Dawnkaski, D. Srivastava and B. J. Garrison, J. Chem. Phys. **104**, 5997 (1996); (b) L. M. Raff, *ibid.* **95**, 8901 (1991); **97**, 7459 (1992); (c) D. C. Sorescu, D. L. Thompson, and L. M. Raff, *ibid.* **102**, 7910 (1995).

[3] D. W. Noid, M. L. Koszykowski, and R. A. Marcus, J. Chem. Phys. **67**, 404 (1977).

[4] R. S. Smith and R. B. Shirts, J. Chem. Phys. **89**, 2948 (1988).

[5] R. S. Dumont and P. Brumer, J. Chem. Phys. **88**, 1481 (1988).

[6] X. Y. Chang, T. D. Sewell, L. M. Raff, and D. L. Thompson, J. Chem. Phys. **97**, 7354 (1992).

[7] W. H. Miller, Phys. Rep. **199**, 124 (1991). This work is an appendix to T. Uzer, *ibid.* **199**, 73 (1991).

[8] K. A. Wood and H. L. Strauss, J. Phys. Chem. **94**, 5677 (1990).

[9] (a) R. Kubo, Adv. Chem. Phys. **15**, 101 (1969); (b) R. Kubo, J. Math. Phys. **4**, 174 (1963).

[10] J. G. Saven and J. L. Skinner, J. Chem. Phys. **99**, 4391 (1993).
[11] R. N. Porter, L. M. Raff, and W. H. Miller, J. Chem. Phys. **63**, 2214 (1975).
[12] For a proof, see E. C. Titchmarsh, *The Theory of the Riemann Zeta-Function*, 2nd ed. (Oxford Science, Clarendon, Oxford, 1986), Lemma 4.2, p. 71.
[13] See, W. Kaplan, *Advanced Calculus* (Addison-Wesley, Cambridge 42, MA, 1953), p. 220.
[14] For a proof, see G. Polya and G. Szego, *Problems and Theorems in Analysis* (Springer, New York, 1972), Vol. 1, Part 3, Problem 205, p. 144.
[15] See, for example, L. M. Raff, J. Chem. Phys. **93**, 3160 (1990).
[16] R. Gunde, P. Gelder and H. H. Gunthard, Chem. Phys. **64**, 313 (1982).
[17] M. E. Riley, M. E. Coltrin, and D. J. Diestler, J. Chem. Phys. **88**, 5934 (1988).
[18] C. C. Chambers and D. L. Thompson, Chem. Phys. Lett. **218**, 166 (1994).
[19] C. C. Martens, M. J. Davis, and G. S. Ezra, Chem. Phys. Lett. **142**, 519 (1987).
[20] J. D. McDonald and R. A. Marcus, J. Chem. Phys. **65**, 2180 (1976).
[21] R. A. Marcus, W. L. Hase, and K. N. Swamy, J. Phys. Chem. **88**, 6717 (1984).